Earthquake Geotechnical Engineering for Protection and Development of Environment and Constructions – Silvestri & Moraci (Eds)
© 2019 Associazione Geotecnica Italiana, Rome, Italy, ISBN 978-0-367-14328-2

Assessment of seismic behavior of deep foundations from large-scale liquefaction shake table experiments

A. Ebeido & A. Elgamal
Department of Structural Engineering, University of California, San Diego, California, USA

ABSTRACT: A series of large-scale 1-g shake-table experiments are conducted to explore the response of single pile and pile-groups due to liquefaction-induced lateral soil deformation. Using the experimental data, insights are drawn and comparisons with current recommendations are made. Furthermore, related three-dimensional finite element (FE) modeling is employed for gleaning further insights. Presence of piles is shown to significantly reduce the extent of accumulated lateral soil deformation. In this regard, high shear strains, additional to those in the free field, occur as the soil moves around the piles in the downslope direction. The associated shear-induced tendency for dilation increases the effective confinement and reduces the resulting downslope deformations. As such, a parametric FE study is undertaken to investigate the effect of soil permeability on this observed liquefaction-induced lateral response. As the prescribed soil permeability increased (in the silt–sand range), higher levels of ground lateral deformation occurred, albeit with a lower pile head displacement and lateral load. Eventually, high permeability (in the gravels range) precluded the accumulation of significant excess pore pressure, with low levels of both soil and pile lateral displacement. On this basis, permeability is highlighted as a critical potentially primary parameter in dictating the effects of liquefaction-induced lateral load on embedded foundation systems

1 INTRODUCTION

Lateral Spreading induced by liquefaction may cause excessive movement and possible failure of pile foundations (e.g., Yasuda & Berrill 2000). This topic is still of high research interest as the slope deformation presents a complex loading situation with the soil undergoing a significant change in its dynamic properties (Finn 2015).

Case history investigations describe a wide range of damage to structures and their pile foundations (e.g., Tokimatsu & Asaka 1998). In the Kobe region, the 1995 Hyogoken-Nambu earthquake was responsible for the damage of many deep foundation supported structures, with failures in steel pipe, precast concrete, and cast-in-place concrete piles. Generally, this damage demonstrated the contribution of both inertial and kinematic forces. Tokimatsu & Asaka (1998) also describe a specific water front structure with deformed pile foundation due to lateral spreading. The kinematic contribution appears throughout the pile's deformed shape with horizontal cracks at the interface between the liquefiable layer and underlying non-liquefiable stratum. This cracking points to local high plastic demands on piles due to the significant difference in soil properties between these layers.

Physical modelling is a valuable resource to complement field investigations. Centrifuge experiments were conducted to study pile kinematic effects during liquefaction and lateral spreading in mildly inclined ground. Studies by Abdoun et al. (2003) and Dobry et al. (2003) in a laminar box with multi-layered soil found the largest bending moment at the interface between liquefied and underlying non-liquefied soil layers. Conclusions from tests by

Brandenberg et al. (2005) show that lateral load direction from different soil layers depends on the incremental and total relative displacement between pile and soil. Brandenberg et al. (2007) further discuss the softening of crust load transfer mechanisms during the passive failure.

In addition to the above, large scale one-g shake table experiments were performed. He (2005), He et al. (2006) and He et al. (2009) discuss four experiments in a mildly inclined laminar box with different single pile and pile group configurations. These experiments address the evolution of pore-water pressures, total pressures and displacements on steel pipe piles along with pile foundation response to such loading. Chang & Hutchinson (2013) tested a reinforced concrete pile in a medium size inclined laminar box and their analysis focused on local plastic demands on the pile and the associated failure mechanism.

Following up on the above efforts, this paper reports the results of a number of additional large-scale experiments. The discussion includes four 5 m soil layer experiments performed on the Japan NIED (He et al. 2006; He et al. 2009) shake table, and 5 experiments on the UCSD medium size shake table (Ebeido 2019). Of the 5 experiments, 4 tests were at 1.80 m soil layer height and 1 test was at 2.90 m soil layer height. All those tests were conducted in mildly inclined laminar container configuration and represent a wide range of testing layouts. The response is analyzed collectively to discuss common results and findings that address the behavior of deep foundations under the conditions of liquefaction-induced lateral spreading.

Experimental results from one of the Japan NIED tests were then employed to calibrate a Finite Element (FE) modeling framework. Comparison with a free field site response scenario (i.e., soil layer without piles) was conducted to highlight the pile restraining effects during this test. Finally, a parametric study (He et al. 2017) was undertaken to investigate the influence of soil permeability on the liquefaction-induced lateral pile response.

2 EXPERIMENTATION PROGRAM

A large number of liquefaction tests are discussed in this document in order to draw insights concerning effect of the resulting lateral spreading on pile foundations. Testing included different soil profiles, different model inclinations and different pile materials. The general objective was to study lateral pile response in layered profiles. A full account is presented in Ebeido (2019).

2.1 *UCSD 1.80 m high experiments*

Figure 1 presents: i) a layout of the 4 experiments conducted using the 1.80 m high medium size laminar box (with inner dimensions of 3.9 m in length and 1.8 m in width), ii) a picture of the laminar box inclined on the shake table, and iii) a top view of the box showing the soil surface for Test 1 just before shaking. As noted by (Law & Lam 2001), the laminar box outside perimeter essentially emulates a periodic boundary condition. Figure 1a illustrates the layout of Test 1 inclined at 2° to the horizontal. The soil profile was a single stratum of loose soil with an estimated relative density of about 20-25% and saturated density of 19 kN/m^3 approximately. The layer was built by sand deposition in water using Ottawa F-65 sand (Bastidas 2016). In order to control the density of the deposited sand, a vibrating mesh was placed to help separate the sand particles and to exercise some control over the deposition velocity. Various mesh positions were used in the other tests to achieve different relative densities. Further details are discussed in Ebeido et al. (2018a). A circular steel pipe pile of 0.25 m diameter and 3 mm thickness was bolted to the box base. Rotational and translational fixity were preferred at the base, though flexibility in the connection allowed for some rotation. This rotational flexibility was assessed via a quasi-static lateral load test to be about 670 kN-m/rad. The pile material is mild steel with 455 MPa yield strength and 2.1x10^5 MPa elastic modulus. At about 66 kN-m, the theoretical yield moment is estimated based on yield stress and section modulus,

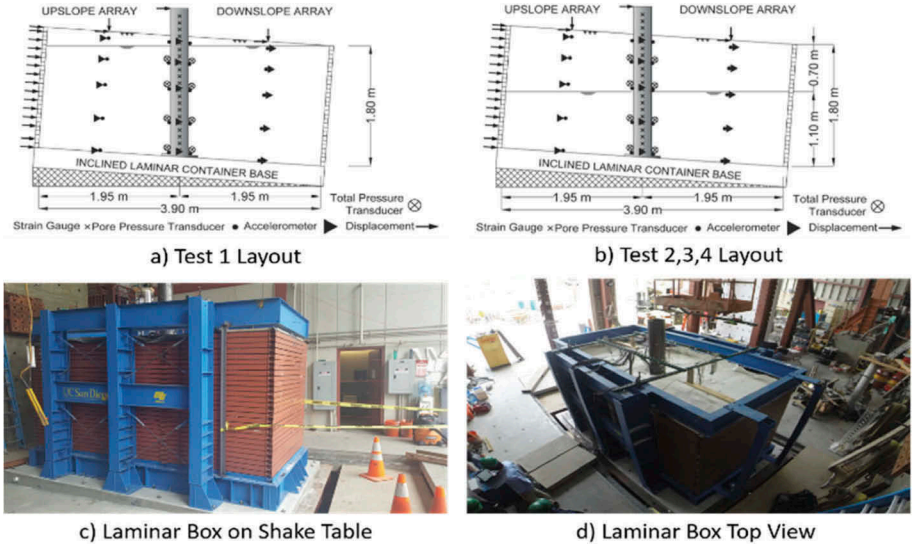

Figure 1. Medium laminar container 1.80 m high test layouts (tests 1-4)

The model was heavily instrumented. Sensors were placed in vertical arrays with dense 20 cm spacing to record the profile response during shaking. A total of 160 sensors were installed with a data collection rate of 256 samples per second.

Pore pressure sensors were deployed on both sides of the pile shaft and in the free soil, midway between the pile and container boundary (upslope and downslope). Pressure transducers were installed on both sides of the pile. An array of ultra-high sampling rate accelerometers was used with the ability to record at 25,000 samples per second (per sensor). Strain gauges were installed on the outside of the steel pipe, with the strains used to back-calculate bending moment during the shaking event. Transducers were mounted on the laminar box exterior wall to measure lateral displacements, and on the soil surface to measure horizontal and vertical displacements. The pile was instrumented as well with transducers to measure pile head displacements above the ground surface.

Figure 1b shows the layouts of Tests 2, 3 and 4. Those tests were variants of Test 1 (Table 1). Test 2 was inclined at 2°, with a lower water table. Water depth was 0.70 m from the downslope surface creating a crust layer on top that was lightly compacted. The top crust layer estimated relative density was 80% while the underlying saturated later relative density was estimated at 50-60%. Test 3 was similar to Test 2 (Ebeido et al. 2018b) with an increase in inclination (4° instead of 2°). Finally, Test 4 was a repetition of Test 3, with a reinforced

Table 1. Summary of experimental program

	Container Dimensions						Cross Section	
Test	Height (m)	Length (m)	Width (m)	Inclination Angle (°)	No. of Sand Layers	Pile Material	Shape	Diameter (m)
1	1.80	3.90	1.80	2	1	Steel	Pipe*	0.25
2	1.80	3.90	1.80	2	2	Steel	Pipe*	0.25
3	1.80	3.90	1.80	4	2	Steel	Pipe*	0.25
4	1.80	3.90	1.80	4	2	Concrete	Circular	0.25
5	2.90	3.90	1.80	4	3	Concrete	Circular	0.25

* 3 mm wall thickness

concrete pile instead of a steel pipe. For Tests 2-4, the top of the bottom layer was horizontal while the top layer was aligned with the slope inclination.

2.2 *UCSD 2.90 m high experiments*

The box height was increased to 2.9 m (Fig. 2 and Table 1) and was inclined at 4° to the horizontal to allow lateral deformation during liquefaction. Figure 3a shows a picture of the box placed on the inclined ramp. The profile height of 2.90 m is divided into 3 sand layers with a single pile in the center as shown in Figure 2. Figure 3b shows the soil surface with the pile in the center after filling. The sand stratum was constructed with a base dense layer, middle loose liquefiable layer and a top dry layer. Similar to the earlier tests, Ottawa F-65 sand (Bastidas 2016) was employed.

The 1.50 m high base layer was constructed by wet sand compaction. Compaction was performed using a plate vibrator in 0.25m lifts achieving a relative density in the range of 80-90% (dense sand), then saturated after compaction. The middle loose layer was 0.70 m high with an estimated soil relative density in the range of 50-60 %. The loose layer sand particles were deposited through water before settling down to help preclude the presence of any trapped air. Finally, the top layer of 0.70m (above the water table) was built with some compaction and an estimated soil relative density in the range of 80-90 %. A top mass was placed on the reinforced concrete pile head to add inertial loading to the kinematic lateral spreading load. Figure 3d illustrates the instrumentation placed on the pile and on the plastic grid supporting the sensor arrays within the soil. The model was subjected to a series of motions, causing the

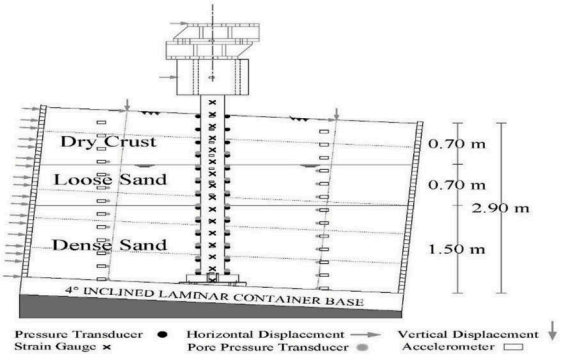

Figure 2. Medium laminar container after extension to 2.90 m high test layout (test 5)

Figure 3. Construction process for test 5 (2.90 m high)

loose layer to liquefy and the soil profile to displace laterally. Total box displacement was nearly 1.00 m causing the reinforced concrete pile to break at its base and lean sideways on the soil. Figure 3e and 3f show the displaced box configuration and the gap formed behind the pile when it tilted forwards. A total of 6 cameras were used to record various aspects of the model during the shaking events.

2.3 *NIED Japan 5.00 m high test program*

Using the large laminar box (Figure 4) at the National Research Institute for Earth Science and Disaster Prevention in Japan (NIED), response of piles subjected to liquefaction-induced lateral spreading was explored (He 2005; He et al. 2006; He et al. 2009). Figure 5 and Table 2 show schematic layouts of the four shake-table experiments. In this testing configuration, the soil container was 11.6 m long, 5.5 m high and 3.5 m wide (inner dimensions) and was inclined at 2° to the horizontal. This inclination corresponds to an infinite slope of about 3° in the field

Figure 4. NIED Japan mildly inclined large laminar container on shake table

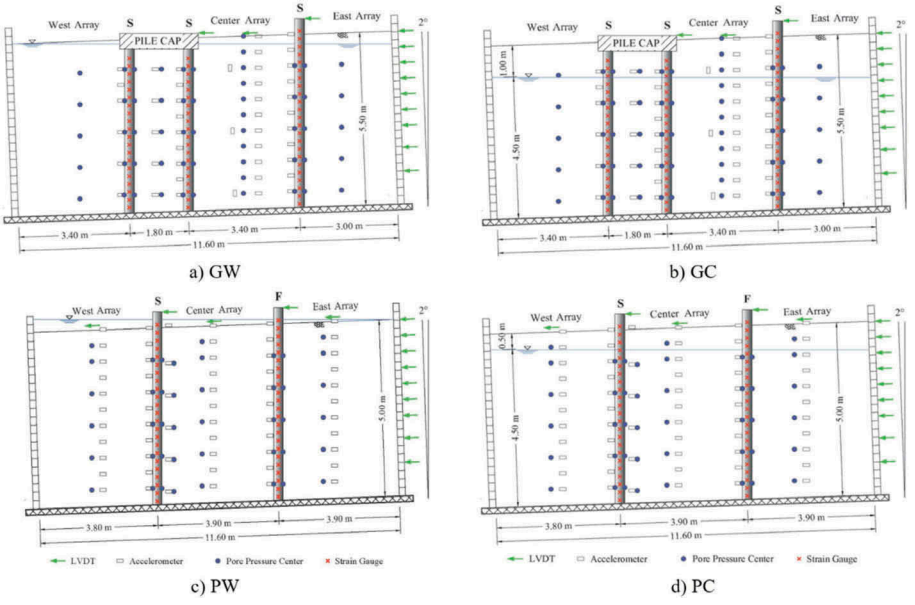

Figure 5. NIED Japan mildly inclined testing configurations

Table 2. Summary of NIED Japan experimental program

	Soil Profile		Pile Properties			
Test	Height (m)	Water table	Diameter (cm)	Wall thickness (cm)	Bending stiffness (kN.m2)	Base Rotational stiffness (kN.m/rad)
GW	5.5	Covers entire soil	31.8	0.6*	14320	18500
GC		1 m below downslope soil				
PW	5.0	Covers entire soil	31.8	0.6*	14320	18500
				0.3**	7360	8500
PC		0.5 m below downslope soil		0.6*	14320	18500
				0.3**	7360	8500

* Denoted in text as stiff pile (S) ** Denoted in text as flexible pile (F)

upon accounting for the laminate weight and water table corrections (Ramirez 2009) following the procedure of Taboada (1995). Input motions for the experiments were in the form of sinusoidal acceleration with a 2 Hz frequency and amplitudes ranging from 0.2-0.3 g.

The soil stratum was constructed by sand deposition in water. Kasumigaura sand (Kagawa et al. 2004) was used with the following grain size characteristics: D_{50} = 0.31 mm, fines content F_c = 3%, and uniformity coefficient C_u = 3. Soil relative density was estimated to be in the range of 40-50 % and saturated density was about 19.4 kN/m^3.

For the configuration of Figure 5a and 5b, the model consisted of a 5.5 m sand layer with a single pile and a 2x2 pile group. The configuration of Figure 5c and 5d consisted of a 5.0 m sand layer and two single piles of different stiffness. In these configurations, water table was near ground surface in one, and well below in the other (to emulate presence of a crust layer).

Table 2 shows characteristics of the soil stratum and pile foundations. Steel pipe piles of 0.318 m (1 ft) diameter were employed in all four experiments, with either a 6 mm (stiff pile) or 3 mm (flexible pile) wall thickness (denoted thereafter as the Stiff "S" and Flexible "F" piles respectively). Plastic moment capacity (Geschwindner 2011) is estimated to be 180 kN-m for the stiff pile and 93 kN-m for the flexible pile. At the container base, the piles mimicked fixity in an assumed underlying firm soil stratum. As such, preliminary static pushover tests were performed on the piles before adding the sand to estimate the attained pile base rotational stiffness values (Table 2).

Each model was instrumented with a large number of accelerometers, pore pressure sensors, total pressure transducers, strain gauges and LVDTs (Figure 5). Instrumentation was placed along the pile shaft and along the profile of the ground stratum. Pore pressure transducers were placed on the piles in addition to being embedded in free field soil. Strain gauges were densely deployed along the pile shaft to aid in back-calculation of bending moment during shaking. Displacement transducers were mounted on the laminar box exterior wall to measure lateral motion, and on the soil surface to measure horizontal and vertical deformation. Furthermore, the piles were instrumented with transducers to measure head displacement above the ground surface.

3 EXPERIMENTATION RESULTS

3.1 *Results of UCSD Test 1*

Input motion for Test 1 shown in Figure 6 was in the form of a sinusoidal acceleration with a 2 Hz frequency (24 cycles) and 0.15g uniform peak amplitude. Due to the imparted base excitation, the excess pore pressure ratio (r_u) presented in Figure 6 show a representative trend. Response shows rapid pore pressure build up reaching liquefaction (r_u = 1) in 1 shaking cycle. Liquefaction appears to occur more or less simultaneously along the layer height.

Instantaneous dips in excess pore pressure for the upslope array are seen to be significantly larger than the downslope array. This can be attributed to soil attempting to dilate as it experiences larger shear strains, while flowing around the pile. The vertical line in these figures denotes the time corresponding to the instant of maximum pile bending moment as will be shown below (Figure 7), occurring at about 1.5 s (about 2 shaking cycles). Maximum moment occurred 1 cycle after liquefaction near the base of the container.

Figure 7 shows the downslope deformation of the soil box and single pile for Test 1. Results show an increase of ground surface displacement with shaking and a resulting accumulated permanent value. Deformations started with shaking and stopped thereafter. Maximum pile head displacement was 11 mm occurring early in the shaking phase, right after liquefaction, at the same instant of the peak bending moment (4.4 kN-m). Soil surface displacement at peak instant was 66 mm with the soil surface continuing to accumulate displacement throughout the shaking event. The final permanent soil deformation was about 306 mm. As the box continued to displace downslope, the soil gradually flowed around the pile (Ebeido 2019) with decrease in pile permanent displacement. At the end of shaking, there was no permanent pile head displacement with a very low residual bending moment (1 kN-m). Peaks in bending

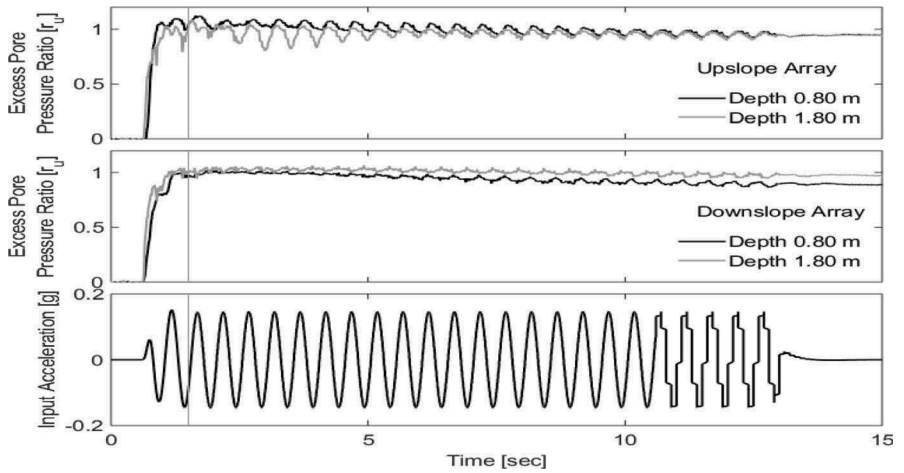

Figure 6. Input shake table acceleration and representative excess pore water pressure ratio time histories (upslope and downslope of the pile for test 1).

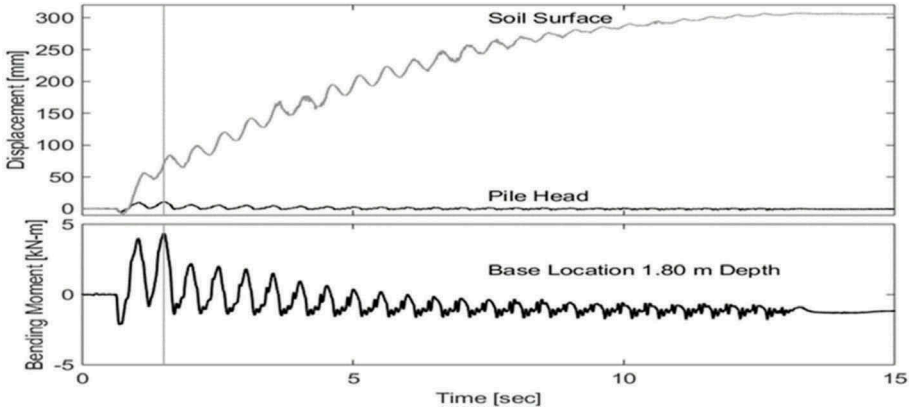

Figure 7. Displacement time histories showing soil surface and pile head and the recorded bending moment at the base for test 1.

moment are seen to correspond to the excess pore pressure transient drops, denoting coincidence with the cyclic large shear strain excursions (Zeghal & Elgamal 1994).

3.2 *Results of Japan NIED test PW*

Figure 5c and Table 2 show the tested configuration with a fully saturated loose layer and 2 single piles of different stiffness. Minimal oscillations in pore water pressure during liquefaction (Fig. 8) suggest the lack of a significant dilative tendency in the liquefied soil response (Zeghal & Elgamal 1994). Bending moment response follows the decay trend discussed in the previous section.

Liquefaction occurs early in the shaking phase as the ground starts to displace incurring pressures on the embedded foundation. After the first few cycles, continued deformation caused no additional permanent displacement or moment in the piles. The box and soil continued displacing reaching as much as 1.00 m (more than 3 pile diameters).

The stiff pile peak response occurred right after liquefaction. Similar to the above UCSD test 1, with the continued loss of soil strength (Ebeido 2019), the soil gradually flowed around the pile causing no additional pressures. Being in its elastic range, the pile eventually fully rebounded back to its starting position.

3.3 *Comparison of different inclinations in UCSD Tests 2 and 3*

Input motion was a 17 s 2 *Hz* sinusoidal wave with gradual increase and decrease in amplitude for Test 2 and 15 s for Test 3. Liquefaction occurred early on, approximately 5.25 s into the shaking phase. Representative time history of excess pore water pressure ratio (Fig. 9) clearly display this mechanism. The vertical line in these figures denotes the time corresponding to the instant of maximum pile bending moment as will be shown below, occurring at about 5.11 s for Test 2 (2°) and 3.12 s for Test 3 (4°) and is included on all time histories for ease of tracking. Maximum moment occurred before liquefaction for both tests at an excess pore pressure ratio of about $r_u = 0.95$ for Test 2 and $r_u = 0.70$ for Test 3.

The general trend of the pore pressure data (Figure 9) displays rapid buildup with instantaneous reductions for both downslope and upslope readings. This indicates some dilative tendency in the liquefied soil response. Instantaneous dips in excess pore pressure for Test 3 are seen to be much larger than those of Test 2. This can be attributed to influence of the increased static driving shear stress in the 4° inclination (Test 3), compared to those of the 2° Test 2.

Figure 10 shows the downslope deformation for the soil box, and single pile for Tests 2 and 3 respectively. Both tests show an increase of ground surface displacement with shaking and a

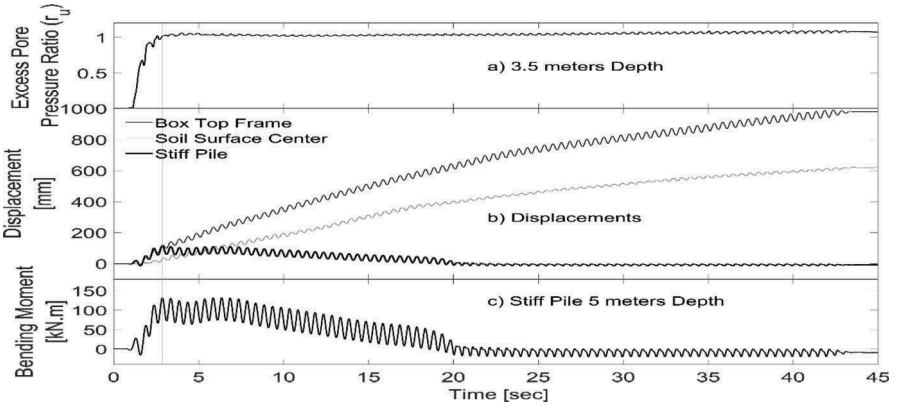

Figure 8. Japan NIED PW Test: a) center array excess pore-pressure (vertical line denotes instance of maximum bending moment), b) displacement time history results, c) stiff pile bending moment, d) flexible pile bending moment.

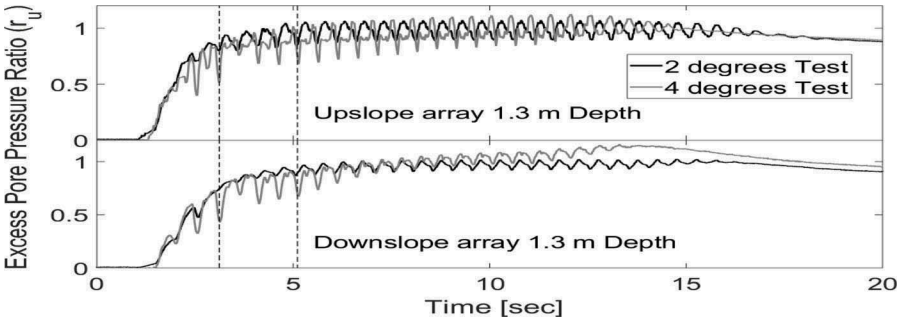

Figure 9. Representative excess pore water pressure ratio time histories for the UCSD tests 2 & 3 at 1.30 m depth (upslope and downslope of the pile).

resulting accumulated permanent value. Deformations started with shaking and stopped thereafter.

In light of the acting initial driving shear stress, it is seen that Test 3 incurred a significantly higher level of deformation earlier during the shaking phase (Figure 10). Of interest as well is that the instant of peak moment on the pile coincided approximately with the same level of ground deformation in both experiments (about 30 mm).

As shaking started, the pile began to oscillate back and forth recording its highest value at the time of maximum bending moment. Values close to maximum displacement were reached before liquefaction, oscillating thereafter around a constant but slightly lower value. Pile head displacement gradually decreased with the ramping down of the input acceleration reaching zero at the end of the shaking event. Absence of permanent pile displacement was a consequence of (Ebeido 2019): i) flow of liquefied soil around the pile, and ii) a gapping mechanism in the upper crust due to a degree of apparent cohesion from compaction moisture-content and capillary action.

Maximum pile head displacement was 16.6 mm and 29.2 mm for Tests 2 and 3 respectively. This shows a 76 % increase in pile head displacement as the inclination changed from 2 to 4 degrees. On the other hand, accumulated ground surface displacement was 19.1 mm and 30.1 mm for Tests 2 and 3 displaying an increase of about 60 %.

Figure 11 shows representative time histories of bending moment at the base of the pile where the maximum values were recorded. Peaks in bending moment are seen to correspond to the excess pore pressure transient drops, denoting coincidence with the cyclic large shear strain excursions (Zeghal & Elgamal 1994). After maximum moment was reached, both tests show oscillation around a constant slightly lower value, gradually decreasing as the shaking was ramped down. As discussed above, both piles rebounded to an almost zero position by the end of shaking, indicating pile linear elastic response. Nevertheless, soil continued to

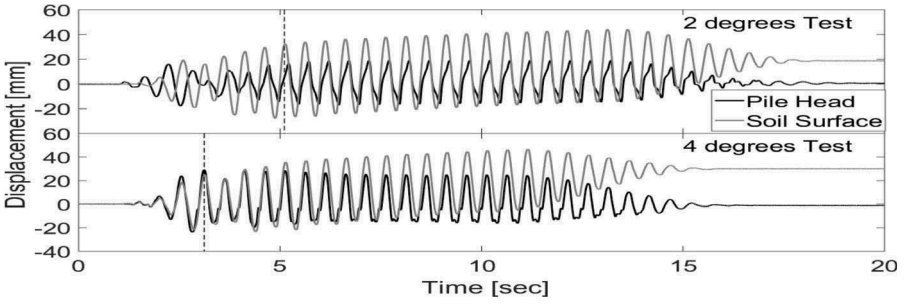

Figure 10. Displacement time histories for the 2 tests showing the soil surface and pile head.

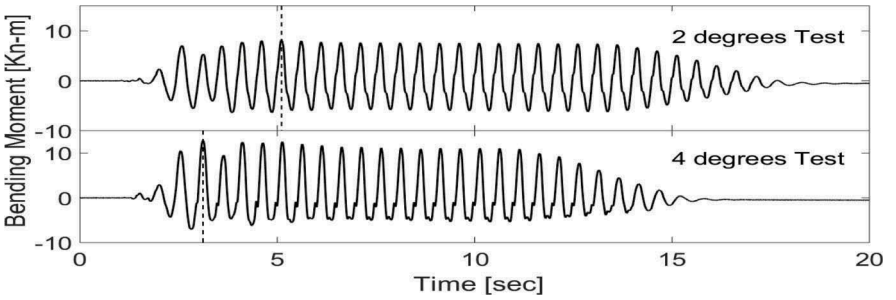

Figure 11. Representative bending moment time histories for the 2 tests at the pile base.

accumulate downslope deformations, after maximum pile response, with no appreciable further pile loading. As such, there was no direct correlation between the final accumulated ground deformation and the observed peak loading on the pile. Brandenberg et al. (2005; 2007) provide further details about the involved crust lateral loading mechanism.

Maximum bending moment recorded for Test 2 was 8 kN-m and 13 kN-m for Test 3 as shown in Figure 11. Therefore, the difference in inclination caused the pile to incur an additional bending moment of about 60 %. Furthermore, maximum response occurred much earlier in the higher 4° inclination test (at 3.12 s) rather than at 5.11 s for 2° experiment. This suggests that the higher inclination caused earlier mobilization of soil movement, just due to pore-pressure increase, but well before the onset of liquefaction.

3.4 *Other general experimental observations*

In addition to the above discussions, the experimental response overall indicated (Ebeido 2019):

i. Accumulated liquefaction-induced deformations are largest near the stratum base (Figure 12a).
ii. In matching the observed early occurrence of peak pile moment, with subsequent reduction as further ground displacement accumulates (Goh & O'Rourke 2008), the liquefied soil lateral spreading *p-y* spring for push over analysis assumes a shape (Ebeido 2019) akin to that proposed for stiff clay (Fig. 12b). In this figure, p is normalized by the pile diameter, D and the liquefied soil residual strength, S_r.

4 FE FRAMEWORK

The FE simulations were conducted using the PEER (Pacific Earthquake Engineering Research Center) FE analysis framework OpenSees (Open System for Earthquake Engineering Simulation). OpenSees is an open source, object-oriented nonlinear FE analysis framework for simulating seismic response of structural and geotechnical systems (McKenna et al. 2010, Mazzoni et al. 2006).

A soil constitutive model based on the multi-yield surface plasticity framework (Prevost 1985) was developed and implemented in OpenSees by Yang et al. (2003). A main objective of this model was to represent the liquefaction-induced cyclic mobility shear strain accumulation mechanism (Parra 1996; Yang 2000; Elgamal et al. 2003; Yang et al. 2002). In this regard, accumulation of permanent deviatoric strain was modeled as a distinct phase within the multi-surface plasticity framework.

This FE framework has been extensively calibrated (Parra 1996; Yang 2000; Elgamal et al. 2003; Yang et al. 2003) for clean Nevada sand with a relative density D_r of about 40%. The calibration phase included the results of monotonic and cyclic laboratory tests (Arulmoli et al.

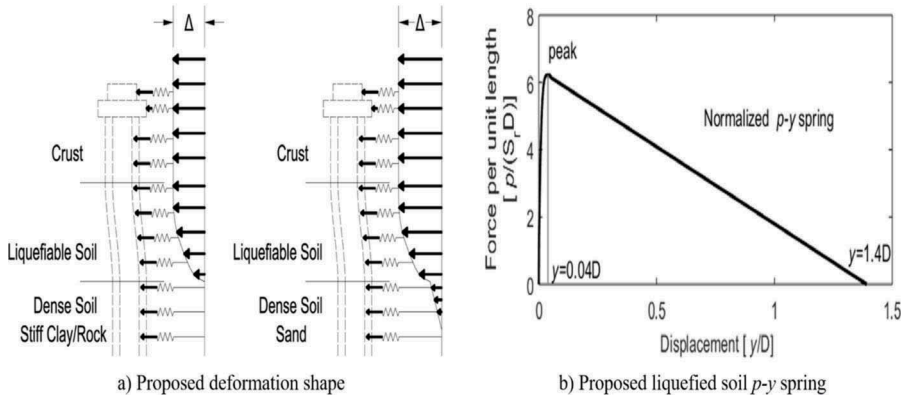

Figure 12. a) Proposed soil profile deformation shapes, b) Proposed liquefied soil *p-y* spring (Ebeido 2019).

1992) and data from dynamic centrifuge-model simulations for both level and infinite mild sloping ground (Dobry & Taboada 1994; Dobry et al. 1995).

The soil domain FE model (Fig. 13) was used to model the NIED Japan experiment referred to as PW (He et al. 2017). For the soil domain, 3D brick elements were used (20-8 node), based on the Chan (1988) u-p formulation (where u is displacement of the soil skeleton, and p is pore pressure) as implemented in OpenSees (Yang & Elgamal 2002; Elgamal et al. 2009). In addition to the damping from hysteresis due to cyclic response, low viscous damping was included (mass proportional term $\alpha_m = 0.0$, and stiffness proportional term $\alpha_k = 0.002$) in order to reduce any potential superfluous noise (Yang & Elgamal 2002; He 2005; Ramirez 2009).

The two piles were modeled using bilinear beam-column elements. Rigid beam-column links, normal to the pile longitudinal axis (Elgamal et al. 2008), were used to represent the geometric space occupied by each pile. The soil domain brick elements were connected to the pile geometric configuration at the outer nodes of these rigid links using the equalDOF constraint in OpenSees for translations only (Law & Lam 2001; Yan 2006; Elgamal et al. 2009). On this basis, the FE model was calibrated using the measured accelerations, displacements,

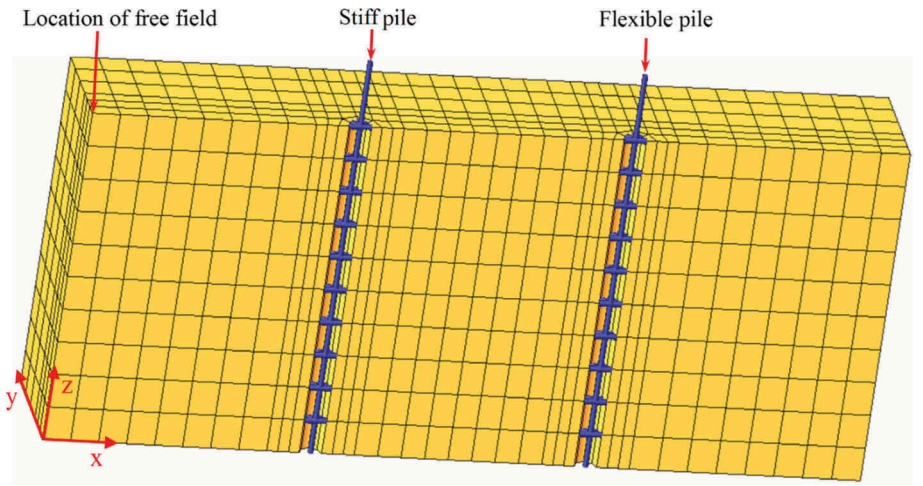

Figure 13. Three-dimensional half mesh (due to symmetry) FE model (Ramirez 2009; He et al. 2017)

excess pore pressures, and the pile head displacements (Ramirez 2009). He et al. (2017) report further details and calibrating modelling parameters.

5 FE ANALYSIS RESULTS

5.1 *Computational parametric study on the effect of changing soil permeability (k)*

To further explore this permeability-related mechanism, additional numerical analyses (Ramirez 2009) were conducted by varying the soil permeability coefficient (k). Along with the benchmark computed scenario (k = 5.0×10^{-5} m/s) the most significant cases studied (Ramirez 2009) were those with higher permeability (i.e., k = 5.0×10^{-4}, 5.0×10^{-3}, and 5.0×10^{-2} m/s). Simulations with lower permeability were also conducted, but these cases followed the general trend that was observed in the benchmark case.

Figure 14 compares time histories of the East-array excess pore pressure for these four permeability cases. Overall, it may be observed that, the higher the permeability, the lower the attained excess pore pressure at greater depths. The soil with the highest permeability (5.0×10^{-2} m/s) did not liquefy, experiencing only some relatively minor excess pore pressure.

Figure 15a displays the soil container displacement after 10 s of shaking. In the liquefied cases, as the permeability increased, the ground displacement is observed to increase. This response mechanism is motivated by the lower attained shear strength resulting from the reduced tendency for negative excess pore pressure (increased effective confinement), particularly in the vicinity of the piles. Eventually, the continued increase in permeability (k = 5.0×10^{-2} m/s) precluded the onset of liquefaction, resulting in a highly diminished permanent ground displacement profile (Fig. 15a).

Figure 15b shows the corresponding stiff pile bending moment profile. As expected, the lowest moments were associated with the highest permeability case that precluded liquefaction and resulted in the least permanent ground deformation. However, for the cases in which the

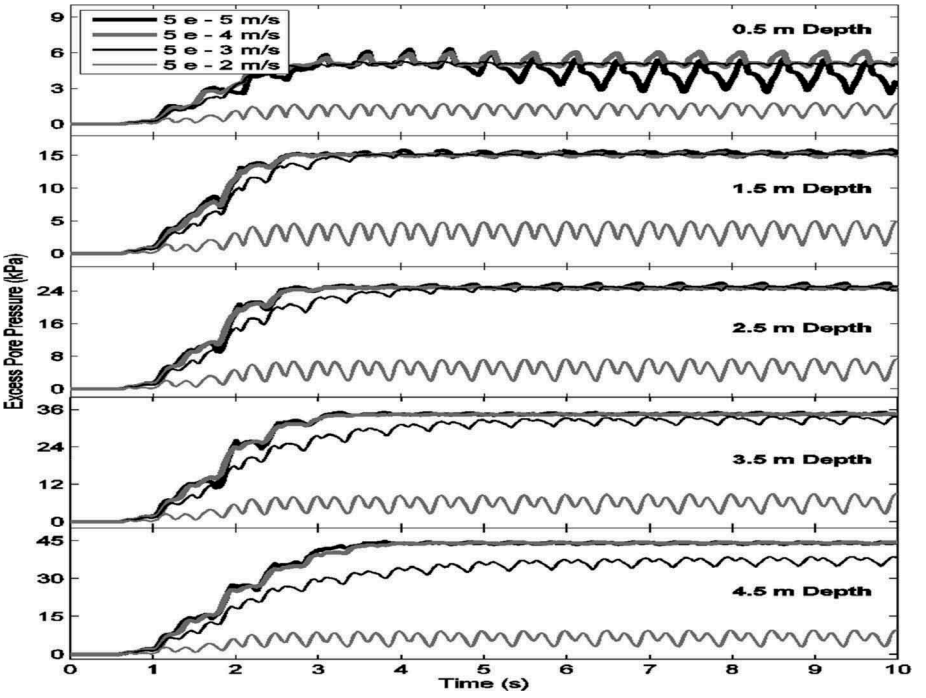

Figure 14. Influence of permeability on the East array excess pore pressures

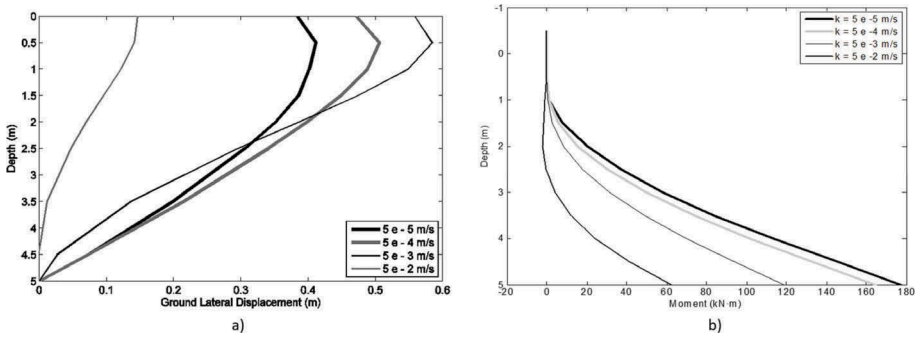

Figure 15. Influence of permeability on: a) the laminar container displacement profile at 10 s, and b) stiff pile moment profile at 10 s

stratum liquefied, the correlation between ground deformation and pile moment suggests (Fig. 15): i) low permeability resulted in the highest moment profile, and the lowest ground surface deformation, and b) as permeability increased, ground surface permanent deformation increased, with a corresponding decrease in the pile moment profile. This inverse correlation between level of ground surface deformation and imposed pile load is directly related to the effect of permeability on the liquefied soil shear-induced dilative response mechanism. In this regard, higher permeability reduces the shear-induced dilative tendency effects, resulting in an overall weaker soil that more easily undergoes lateral permanent deformation; thus promoting downslope flow around the pile and reducing the imposed lateral load.

5.2 *Pile restraining effect on lateral deformations*

The above discussion as relates to the pile-ground shear-induced dilative tendency mechanism, suggests that presence of the piles hinders the downslope accumulation of ground deformations. To assess the extent of this pile restraining effect, an additional numerical simulation of the benchmark model was conducted without inclusion of the piles (essentially representing a free-field scenario). The resulting excess pore pressures and acceleration (Fig. 16) were essentially similar to those of the benchmark response (He et al. 2017). However, displacement in the absence of piles (Fig. 16) was significantly larger than the corresponding experimental values, in excess of 1.8 m at the ground surface, compared to the 0.4 m with the piles. This large contrast in accumulated displacement should be taken only as indicative of the possible restraining effects in a large-scale deployment of such piles, with the soil container essentially constituting a sort of periodic boundary condition (Law & Lam 2001).

6 CONCLUSIONS

A number of large scale 1-g shaking table tests were performed at University of California, San Diego and NIED, Japan to study pile foundation response during liquefaction-induced lateral spreading. Tests had different inclinations, soil profiles, and heights and pile materials/cross-sections. The model configurations are described along with the deployed dense instrumentation. Sinusoidal input motions were chosen for the testing program. Such large-scale 1-g tests are time consuming and costly, but allow for insights derived from possible presence of dense instrumentation and use of reinforced concrete pile construction materials.

From this particular data set it may be concluded that:

i. values approaching peak bending moment were noted quite early in the shaking phase. Increased lateral spreading due to the continued soil downslope deformation, did not result in appreciable increase in pile displacements or moments.

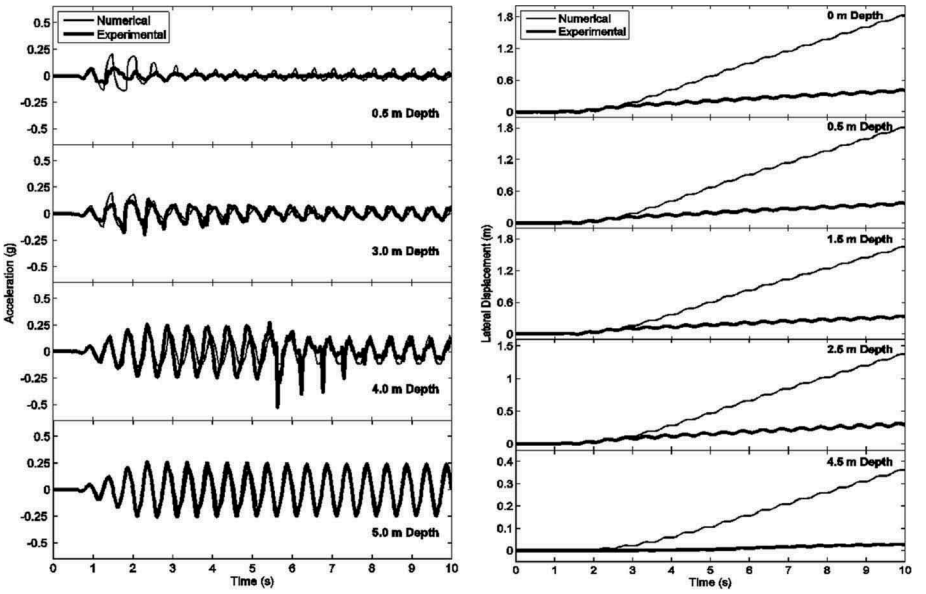

Figure 16. Calibrated model (He et al. 2017) numerical response of the ground system without the piles, compared to the recorded experimental data with the piles: a) acceleration, and b) displacement

ii. as the driving static shear stress increases, it is likely that peak moment will occur earlier, with excess pore pressures that might be well below those corresponding to the onset of liquefaction.
iii. Comparing the different inclinations between tests 2 and 3, we find that the pattern of pile response is similar in both cases as indicated by the measured bending moment and displacements. However, the increase in ground inclination caused an additional 60 % in bending moment and 76% in pile head displacement. The higher locked-in driving shear stress in the 4-degree scenario triggered the crust to start moving earlier, with lower excess pore pressure ratio r_u= 0.70 (rather than at r_u= 0.95 for the 2-degree scenario).
iv. In general, maximum bending moments were significantly lower than numerical predictions by conventional practical approaches (Ebeido 2019).

From the presented FE analysis results, the main findings were:

i. additional large shear strains occurred as the soil moved around the piles towards the downslope direction. The associated shear-induced dilative tendency had a restraining effect on the ground response, thus significantly reducing the permanent lateral laminar container deformations.
ii. Increasing the soil permeability weakened the dilative tendency-induced instants of regain in soil shear stiffness and strength, increasing the free-field displacements, and decreasing the pile displacements/moments. In the investigated scenario, permeability values corresponding to a soil D_{10} of about 0.5 mm and larger were quite effective in achieving this outcome.

ACKNOWLEDGEMENTS

The presented research conducted at UCSD is supported by the California Department of Transportation with Dr. Charles Sikorsky as the Program Manager. This support is gratefully

acknowledged. The authors would like to thank the staff and research engineers of the UCSD Powell laboratories. Partial contribution by Kyowa Americas Inc. to the soil pressure and pore pressure transducers employed at UCSD and their technical support is gratefully appreciated. The NIED Japan research was partially supported by the Pacific Earthquake Engineering Research Center (PEER) Lifeline Program (Mr. Thomas Shantz), and the National Science Foundation (award number CMMI-1201195). The mildly inclined laminar container test configuration was patterned after earlier centrifuge studies conducted by Professors Ricardo Dobry and Tarek Abdoun at the Rensselaer Polytechnic Institute. Under the oversight of Professor Tokimatsu, the experiments using the large laminar container were conducted at the National Research Institute for Earth Science and the Disaster Prevention (NIED) laboratory in Tsukuba, Japan (in conjunction with Dr. Akio Abe and Dr. Masayoshi Sato). Finally, follow up studies included significant additional contributions by Dr. Liangcai He, Mr. Jose Ramirez, Dr. Jinchi Lu, Mr. Thomas Shantz, Dr. Jorge Meneses, and Professor Liang Tang.

REFERENCES

Abdoun, T., Dobry, R., O'Rourke, T. D. & Goh, S. H. (2003). Pile response to lateral spreads: centrifuge modeling. *Journal of Geotechnical and Geoenvironmental Engineering* 129(10),869–878.

Arulmoli, K., Muraleetharan, K. K., Hossain, M. M., & Fruth, L. S. (1992). *VELACS: Verification of liquefaction analyses by centrifuge studies, laboratory testing program*. Soil Data Report, Project No. 90-0562, the Earth Technology Corporation, Irvine, CA.

Bastidas, A. M. (2016). *Ottawa F-65 Sand Characterization*. Ph.D Dissertation, University of California, Davis.

Brandenberg, S. J.; Boulanger, R. W.; Kutter, B. L.; & Chang, D. (2005). Behavior of pile foundations in laterally spreading ground during centrifuge tests. *Journal of Geotechnical and Geoenvironmental Engineering*. 131(11),1378–1391.

Brandenberg, S. J.; Boulanger, R. W.; Kutter, B. L.; & Chang, D. (2007). Liquefaction-Induced Softening of Load Transfer between Pile Groups and Laterally Spreading Crusts," *Journal of Geotechnical and Geoenvironmental Engineering*, 133(1),91–103.

Chan, A. H. C. (1988). "*A unified finite element solution to static and dynamic problems in geomechanics*." Ph.D. thesis. University College of Swansea, U.K.

Chang, B. J., & Hutchinson, T. C. (2013). Experimental investigation of plastic demands in piles embedded in multi-layered liquefiable soils. *Soil Dynamics and Earthquake Engineering* 49, 146–156.

Dobry, R., & Taboada, V. M. (1994). "Possible lessons from VELACS model No. 2 results." *Proc. Intl. Conf. on Verification of Numerical Procedures for the Analysis of Soil Liquefaction Problems*, K. Arulanandan & R. F. Scott, eds., Balkema, Rotterdam, The Netherlands, 2, 1341–1352.

Dobry, R., Taboada, V. M., & Liu, L. (1995). "Centrifuge modeling of liquefaction effects during earthquakes." Keynote Lecture, *Proc., 1st Int. Conf. on Earthquake Geotechnical Engineering (IS-Tokyo)*, K. Ishihara, ed., Balkema, Rotterdam, the Netherlands, 3, 1291–1324.

Dobry, R., Abdoun, T., O'Rourke, T. D. & Goh, S. H. (2003). Single piles in lateral spreads: Field bending moment evaluation. *Journal of Geotechnical and Geoenvironmental Engineering*. 129(10),879–889.

Ebeido, A., Zayed, M., Kim, K., Wilson, P., & Elgamal, A., (2018a). Large Scale Geotechnical Shake Table Testing at the University of California San Diego. *Proc. of the 2nd GeoMEast International Congress and Exhibition on Sustainable Civil Infrastructures*. Cairo, Egypt. 24-28 November.

Ebeido, A., Elgamal, A., & Zayed, M., (2018b). Pile response during liquefaction-induced lateral spreading: 1-g shake table tests with different ground inclination. *Proc. 9th international conference on Physical Modelling in Geotechnics*. City, University of London. 17-20 July.

Ebeido, A. (2019). *Lateral-Spreading Effects on Pile Foundations: Large-scale Testing and Analysis*. PhD Thesis. Department of Structural Engineering. University of California San Diego, La Jolla, CA.

Elgamal, A., Yang, Z., Parra, E., & Ragheb, A. (2003). "Modeling of cyclic mobility in saturated cohesionless soils." *International Journal of Plasticity*, 19(6),883–905.

Elgamal, A., Yan, L., Yang, Z., & Conte, J. P. (2008). "Three-dimensional seismic response of Humboldt bay bridge-foundation-ground system." *J. Structural Eng*., ASCE, 134, 7, 1165–1176.

Elgamal, A., Lu, J., & Forcellini, D. (2009). "Mitigation of liquefaction-induced lateral deformation in a sloping stratum: three-dimensional numerical simulation." *Journal of Geotechnical and Geoenvironmental Engineering*, 135, 11, 1672–1682.

Finn, W. L. (2015). 1st Ishihara Lecture: An over- view of the behavior of pile foundations in liquefiable and non-liquefiable soils during earthquake excitation. *Soil Dynamics and Earthquake Engineering*. 68, 69–77.

Geschwindner, L. F. (2011). *Unified design of steel structures*. Wiley Global Education.

Goh, S. H., & O'Rourke, T. D. (2008). Soil-pile interaction during liquefaction-induced lateral spread. *Journal of Earthquake and Tsunami*, 2(01), 53–85.

He, L. (2005). Liquefaction-induced lateral spreading and its effects on pile foundations. Ph.D Dissertation, University of California, San Diego.

He, L., Elgamal, A., Abdoun, T., Abe, A., Dobry, R., Meneses, J., Sato, M. & Tokimatsu, K. (2006). Lateral loads on piles due to liquefaction induced lateral spreading during one-g shake table experiments. *Proceedings of the 8th U.S. National Conference on Earthquake Engineering*, San Francisco, CA.

He, L., Elgamal, A., Abdoun, T., Abe, A., Dobry, R., Hamada, M., Menses, J., Sato, M., Shantz, T., & Tokimatsu, K. (2009). Liquefaction-Induced Lateral Load on Pile in a Medium Dr Sand Layer, *Journal of Earthquake Engineering*. 13:7, 916–938.

He, L., Ramirez, J., Lu, J., Tang, L., Elgamal, A., & Tokimatsu, K. (2017). Lateral spreading near deep foundations and influence of soil permeability. *Canadian Geotechnical Journal*, 54(6), 846–861.

Kagawa, T., Sato, M., Minowa, C., Abe, A., & Tazoh, T. (2004). Centrifuge simulations of large-scale shaking table tests: Case studies, *Journal of Geotechnical and Geoenvironmental Engineering* 130(7), 663–672.

Law, H. K. & Lam, I. P. (2001). Application of periodic boundary for large pile group, *Journal of Geotechnical and Geoenvironmental Engineering* 889–892.

Mazzoni, S., McKenna, F., & Fenves, G. L. (2006). "*Open system for earthquake engineering simulation user manual*." Pacific Earthquake Engineering Research Center, University of California, Berkeley.

McKenna, F., Scott, M., & Fenves, G. (2010). "Nonlinear Finite-Element Analysis Software Architecture Using Object Composition." *J. Comput. Civ. Eng*., 24(1), 95–107

Parra, E. (1996). "*Numerical modeling of liquefaction and lateral ground deformation including cyclic mobility and dilation response in soil systems*." Ph.D. thesis, Rensselaer Polytechnic Institute, Troy, NY.

Prevost, J. H. (1985). "A simple plasticity theory for frictional cohesionless soils." *Soil. Dyn. Earthquake Eng*., 4(1), 9–17.

Ramirez, J. M. (2009). *Influence of Soil Permeability on Liquefaction-Induced Lateral Pile Response*. M.S. thesis, Department of Structural Engineering, University of California, San Diego, CA.

Taboada, V. M. (1995). "*Centrifuge modeling of earthquake-induced lateral spreading in sand using a laminar box*." Ph.D. thesis, Civil Engineering Dept., Rensselaer Polytechnic Institute, Troy, NY.

Tokimatsu, K. & Asaka, Y. (1998). Effects of Liquefaction-Induced Ground Displacements on Pile Performance in the 1995 Hyogoken-Nambu Earthquake. *Soils and Foundations*, Special Issue, pp. 163–177.

Yan, L. (2006). "*Sensor data analysis and information extraction for structural health monitoring*," PhD Thesis, Dept. of Structural Engng, University of California, San Diego, La Jolla, CA.

Yang, Z. (2000). "*Numerical modeling of earthquake site response including dilation and liquefaction*." Ph. D. thesis. Columbia University, New York, NY.

Yang, Z., & Elgamal, A. (2002). "Influence of permeability on liquefaction-induced shear deformation." *Journal of Engineering Mechanics*, ASCE, 128(7), 720–729.

Yang Z., Elgamal A., and Parra E. (2003). "A computational model for cyclic mobility and associated shear deformation." *J. Geotech. and Geoenviron. Eng*., 129(12), 1119–1127.

Yasuda, S. & Berrill, J.B. (2000). Observations of the Earthquake Response of Foundations in Soil Profiles Containing Saturated Sands. *1st International Conference on Geotechnical and Geological Engineering*. Melbourne, Australia, Issue Lecture, pp. 1441–1471.

Zeghal, M. & Elgamal, A.-W. (1994). Analysis of site liquefaction using earthquake records. *Journal of Geotechnical Engineering* 120(6), 996–1017.